BIOCHEMISTRY
including biophysical chemistry & molecular biology

Article

pubs.acs.org/biochemistry

Mechanism of Autophosphorylation of Mycobacterial PknB Explored by Molecular Dynamics Simulations

Nikhil P. Damle and Debasisa Mohanty*

Bioinformatics Center, National Institute of Immunology, Aruna Asaf Ali Marg, New Delhi 110067, India

Supporting Information

ABSTRACT: Mycobacterial Ser/Thr kinase, PknB, is essential for the growth of the pathogen. Unphosphorylated PknB is catalytically inactive, and its activation requires autophosphorylation of Thr residues on the activation loop. Autophosphorylation can in principle take place via two distinct mechanisms. Intermolecular trans autophosphorylation involves dimerization and phosphorylation of the activation loop of one chain in the catalytic pocket of the other chain. On the other hand, intramolecular cis autophosphorylation involves phosphorylation of the activation loop of the kinases in its own catalytic pocket within a monomer. On the basis of the crystal structure of PknB in the front-to-front dimeric form, it is currently believed that activation of PknB involves trans autophosphorylation. However, because of the lack of coordinates of the activation loop in the crystal structures, atomic details of the conformational changes associated with activation are yet to be deciphered. Therefore, to understand the conformational transitions associated with activation via autophosphorylation, a series of explicit solvent molecular dynamics simulations with a duration of 1 μs have been performed on each of the phosphorylated and nonphosphorylated forms of the PknB catalytic domain in monomeric and dimeric states. Simulations on phosphorylated PknB revealed a differential network of crucial electrostatic and hydrophobic residues that stabilize the phosphorylated form in the active conformation. Interestingly, in our simulations on nonphosphorylated monomers, the activation loop was observed to fold into its own active site, thereby opening the novel possibility of activation through intramolecular cis autophosphorylation. Thus, our simulations suggest that autophosphorylation of PknB might also involve cis initiation followed by trans amplification as reported for other eukaryotic kinases based on recent reaction kinetics studies.

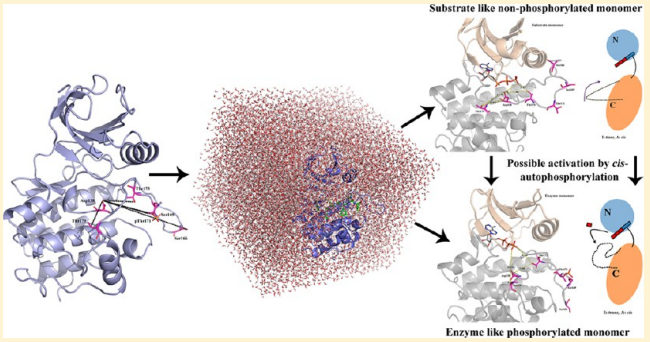

PknB is one of the 11 eukaryotic like Ser/Thr kinases in *Mycobacterium tuberculosis* and is essential for the pathogen's growth.[1,2] The PknB polypeptide consists of an N-terminal intracytoplasmic kinase catalytic domain linked to a transmembrane domain by a short juxtamembrane region. Peptidoglycan fragments from periplasmic space are believed to bind to the C-terminal extracytoplasmic PASTA domains of PknB and activate its catalytic domains through ligand-induced dimerization.[3,4] Several crystal structures of the PknB catalytic domain are available, in both monomeric and dimeric states.[5−7] The catalytic kinase domain of PknB (KD) shows a well-conserved kinase fold with a bilobal architecture.[8] Various experimental studies have revealed that unphosphorylated PknB is catalytically inactive and autophosphorylation of threonines in the activation loop is necessary for activation of PknB.[9−11] Of the five phosphorylatable residues in the activation loop of PknB, residues Thr171 and Thr173 have been shown to be the primary and secondary autophosphorylation sites *in vivo*.[12] However, biochemical and mass spectrometric (MS) data also suggest phosphorylation of Ser169 and Thr179 residues in the activation loop.[6,10] Several experimental studies have attempted to decipher the mechanistic details of the autophosphorylation in the activation loop and consequent activation of PknB. Figure 1 summarizes the currently accepted model for activation that has emerged from crystallographic, biochemical, and other *in vivo* experiments.

This model for autophosphorylation of the PknB activation loop invokes two different modes of ligand-induced dimerization resulting from binding of muropeptides to extracellular PASTA domains.[13,14] Crystallographic structures are available for the PknB catalytic domain in monomeric form as well as in two distinct modes of dimerization, i.e., back-to-back dimer and front-to-front dimer.[6,7,11] The N-lobe-mediated back-to-back dimerization induces an activelike conformation in the monomeric subunits, and one such back-to-back dimer phosphorylates another by formation of a front-to-front dimeric interface.[13] In this proposed mode of autophosphorylation, the activation loop of the substratelike subunit is oriented toward the catalytic pocket of the enzymelike subunit. Thus, this mode of autophosphorylation of PknB is essentially intermolecular trans autophosphorylation involving asymmetric front-to-front

Received: February 25, 2014
Revised: June 27, 2014
Published: July 2, 2014

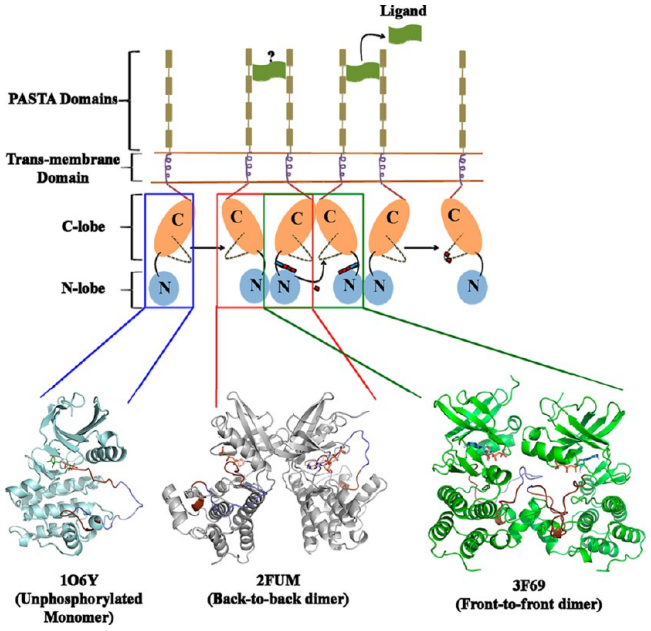

Figure 1. Model proposed in the literature for activation of PknB by autophosphorylation (top), which invokes formation of two different modes of PknB dimerization, viz., back-to-back and front-to-front, colored red and green, respectively. Different segments of the PknB polypeptide are appropriately labeled. The unphosphorylated monomer is shown as a blue box. The bottom panel indicates the available crystal structures for the respective forms of the PknB catalytic domain. In the crystal structures, the part of the activation segment that was present in crystal structures is colored brown and the part that was missing and hence modeled is colored blue.

dimerization. In the front-to-front dimeric crystal structure of the PknB catalytic domain, the enzymelike chain is phosphorylated at primary autophosphorylation site Thr171 and the activation loop of the substratelike nonphosphorylated chain is oriented toward the catalytic pocket of the phosphorylated chain.[6] Interestingly, the crystal structure of a similar trans autophosphorylation complex involving an asymmetric homodimer has also been elucidated for p21-activated protein kinase, PAK1.[15] Therefore, it is currently believed that activation of PknB involves an intermolecular trans autophosphorylation similar to that of PAK1.

However, the crystal structure of front-to-front dimer of the PknB catalytic domain lacks the coordinates of several residues in the activation loops of the enzymelike and substratelike chains, as they were disordered. Therefore, it is not apparent from the available crystal structure how phosphorylation at Thr171 locks one chain in the enzymelike conformation and how exactly the nonphosphorylated activation loop reaches the γ-phosphate of ATP in the enzymelike chain. In principle, molecular modeling of the conformations of missing residues and molecular dynamics simulations of the modeled dimeric complexes in an explicit solvent environment can reveal mechanistic details of intermolecular trans autophosphorylation at the atomic level.

Second, a detailed examination of various steps involved in the activation of PknB indicates that, for the formation of the asymmetric front-to-front dimer, it would be necessary that at least one chain of the back-to-back dimer be phosphorylated and that such a phosphorylation stabilize the enzymelike conformation. Because in the back-to-back dimer the activation segments and catalytic pockets of each chain are oriented away from each other, the phosphorylation of the activation loop would per se involve intramolecular cis autophosphorylation within a single monomer. It is possible that allosteric interactions from N-lobe-mediated dimerization might help in inducing this cis autophosphorylation. Interestingly, it has recently been demonstrated by detailed analysis of reaction kinetics that autoactivation of PAK2 involves intramolecular cis initiation followed by amplification through trans autophosphorylation involving dimerization.[16] Similarly, on the basis of the crystal structure of domain-swapped dimers, it was proposed that autoactivation of other kinases like Chk2 and Aurora-A follows intermolecular trans autophosphorylation. However, recent kinetic analyses suggest an intramolecular cis autophosphorylation mechanism for these two kinases.[17] Therefore, it is possible that similar to the case for PAK2, Chk2, and Aurora-A, initiation of autophosphorylation in PknB also takes place within the monomeric chain via the intramolecular cis autophosphorylation mechanism. This activation mechanism is possibly aided by allosteric interactions resulting from formation of back-to-back dimers, and in the next step, autophosphorylation is further enhanced through trans autophosphorylation involving formation of the asymmetric front-to-front dimer. This mode involves association of a phosphorylated enzymelike chain with a nonphosphorylated substratelike chain. Hence, it would also be interesting to explore the conformational feasibility of intramolecular cis autophosphorylation within a monomer of PknB by using molecular dynamics simulations. Comparisons of the conformations of different chains in back-to-back and front-to-front dimers as well as monomeric PknB (Figure S1 of the Supporting Information) indicate that they differ primarily in the conformations of activation loops and also in terms of the subtle reorientation of the N-lobe with respect to the C-lobe. Therefore, it might be possible to sample the conformational changes associated with cis and trans autophosphorylation by performing long explicit solvent MD simulations.

Hence, in this study, we have performed 1 μs explicit solvent MD simulations on the asymmetric front-to-front dimer of PknB and also on the phosphorylated and nonphosphorylated forms of monomeric PknB. The main objectives of this study are to elucidate the conformational changes associated with intermolecular trans autophosphorylation of PknB and to explore the conformational feasibility of intramolecular cis autophosphorylation in monomeric PknB. Our simulations have revealed the structural basis of stabilization of the active conformation by phosphorylation of the activation loop. In our simulations, the activation loop of the monomer was observed to fold into its own active site, thereby opening a previously unexplored possibility of intramolecular cis autophosphorylation for PknB. Interestingly, phosphorylation of the primary autophosphorylation site (Thr171) was found to facilitate conformational transitions of the activation loop in such a way that the secondary autophosphorylation site (Thr173) is brought into the vicinity of the active site of the same monomer. Thus, our results suggest the possibility of cis autophosphorylation through a novel cooperative effect.

MATERIALS AND METHODS

Selection of Starting Structures for Simulations. The crystal structure of the *M. tuberculosis* PknB mutant protein [Protein Data Bank (PDB) entry 3F69] was selected as the starting structure for the simulations on the dimer in the front-to-front mode.[6] The Thr171 residue in chain B of this dimeric

PknB was phosphorylated; hence, this chain acts as an enzymelike chain of the dimer, while chain A that lacks phosphothreonine at position 171 acts as a substrate. For the sake of convenience, the enzymelike chain of dimeric PknB will be termed dimer_E and the substratelike chain dimer_S. Apart from the simulations of the dimer, to study the dynamic behavior of phosphorylated and nonphosphorylated forms of monomeric PknB structures, the phosphorylated and nonphosphorylated chains of the front-to-front PknB dimer were taken apart and simulations were performed on each of them in isolation in the solvent environment. Again for the sake of convenience, the phosphorylated and nonphosphorylated monomer chains will be termed monomer_E and monomer_S, respectively (Table 1). The crystal structure of the PknB front-to-front dimer had bound Mg^{2+}, but instead of ATP, it had been determined in complex with eukaryotic kinase inhibitor KT5720. However, PDB entry 1O6Y, the monomeric structure of PknB,[5] was available in complex with phosphomethyl phosphonic acid adenylate ester (ACP), which differs from ATP in terms of the presence of a carbon atom in place of β-oxygen that connects the β-phosphate to γ-phosphate. Therefore, ATP- and Mg^{2+}-bound structures were modeled for dimeric and monomeric PknB by transforming the coordinates of ACP after optimal superposition of 1O6Y on each chain of dimeric PknB. The transformed ACP was subsequently converted to ATP by replacing the carbon atom with oxygen. Figure S2 of the Supporting Information shows the superposition of the KT5720-bound structure of PknB on the structure where ATP has been modeled in the inhibitor binding site. As can be seen, the side chains adopt a very similar conformation, indicating appropriate modeling of ATP in the binding site. The coordinates for residues 164−178 in the activation loop of the nonphosphorylated chain and residues 174−176 on the phosphorylated chain were not available in the dimeric structure of PknB as the corresponding regions were disordered. Modeller9v8[18] was used to model the coordinates of a three-residue stretch (174−176) on the phosphorylated chain and a 15-residue stretch (164−178) on the nonphosphorylated chain of PknB dimer crystal structure 3F69. A set of 10 models corresponding to multiple low-energy states were generated. Modeller scored them using molecular probability density function (molpdf) values that are essentially a sum of restraint energies. Figure S3 of the Supporting Information shows the superposition of these 10 models. Even though these models had similar molpdf values in the range of 2631−3030, they mainly differed in the orientation of the 15-residue stretch in the activation loop of the nonphosphorylated chain. On the other hand, the three-residue stretch modeled in the phosphorylated chain had almost identical conformations in all 10 models. The dimer model (indicated by the arrow in Figure S3 of the Supporting Information) that had a Ser/Thr residue in the activation loop of the nonphosphorylated chain closest to the catalytic Asp138 of the phosphorylated chain was selected for MD simulations. The phosphorylated chain of this dimer model was selected as the initial structure for the enzymelike monomer (monomer_E) simulation, while the initial structure for the substratelike monomer (monomer_S) was derived from monomer_E after converting pThr171 to Thr.

Table 1. Various Systems Simulated in This Study and Their Respective Simulation Lengths

system	description	simulation length	
		AMBER	GROMACS
dimer	3F69 dimer (chain B with pThr171)	1 μs	100 ns
monomer_E	enzyme monomer (chain B with pThr171)	1 μs	100 ns
monomer_S	substrate monomer (chain B with Thr171 instead of pThr171)	1 μs	100 ns

Simulation Setup. The monomeric and dimeric structures of PknB were provided as input to the xleap module of the AMBER 11 simulation package[19] for obtaining coordinate and topology files for molecular dynamics simulations. Molecular mechanics parameters were assigned using the ff03 force field.[20] Charges and other parameters for phosphothreonine (pThr), ATP, and Mg^{2+} were taken from the AMBER parameter database[21−23] developed by the Bryce group (http://www.pharmacy.manchester.ac.uk/bryce/amber). Prior to the initiation of MD simulations, energy minimization was conducted in two stages. Initially, the crystal structures with modeled activation loop regions were minimized in vacuum to remove steric clashes, if any. In the second stage, the structures were solvated using the simple point charge extended (SPCE) water[24] model in an octahedral box, with box edges lying 10 Å from the outermost atoms of the proteins in all directions. The overall charge on the system was neutralized, and the entire solvated system was minimized using the steepest descent approach for a maximum of 100000 cycles with a convergence criterion of 0.0001 kcal mol^{-1} $Å^{-1}$. The solvated PknB dimer consisted of 42430 atoms in total, including 11197 solvent molecules, four Mg^{2+} ions, and two ATPs, while monomeric forms of PknB had approximately 25000 atoms in total, including around 6900 water molecules along with two Mg^{2+} ions and an ATP each. MD simulations were conducted using a time step of 2 fs, and bonds containing hydrogens were constrained using SHAKE.[25] For each of the three simulations, the systems were heated to 300 K during a 20 ps dynamics simulation using the *NVT* ensemble. The temperature of the system was constrained using Langevin dynamics temperature coupling and a collision frequency of 2 ps^{-1}. The advantage of temperature control in explicit solvent simulations by Langevin dynamics over simple velocity scaling is that it ensures a uniform temperature distribution over all parts of the molecule and stabilization of the MD integrator even at longer time steps.[26] Later pressure was equilibrated to 1 atm over a period of 100 ps using isotropic position scaling and keeping the temperature constant at 300 K. After a stable density (∼1 g cm^{-3}) and a stable temperature (∼300 K) had been ensured, a production MD run was conducted using the *NPT* ensemble for 1 μs at 300 K and 1 atm for each of the three systems. All the three simulations were performed using periodic boundary conditions, and long-range electrostatics interactions were computed using the particle mesh Ewald (PME) summation method[27] using a cutoff of 12 Å in direct space. The van der Waals interactions were also computed using a cutoff of 12 Å. All the MD simulations were performed using sander and a parallel CUDA version of PMEMD from AMBER 11. After completion of the initial 500 ns, the MD simulations were extended up to 1 μs using the same ff03 force field and CUDA version of PMEMD from AMBER 12. Simulations for 100 ns each were also performed on all three systems, namely, dimer, monomer_E, and monomer_S, in GROMACS by using the GROMOS force field (G43a1).[28] Results from AMBER and GROMACS simulations showed similar trends. Hence, results

dx.doi.org/10.1021/bi500245v | *Biochemistry* 2014, 53, 4715−4726

from longer AMBER MD simulations of 1 μs have been discussed in detail. A brief analysis of a comparison of results from GROMACS and AMBER simulations is also provided.

Analysis of MD Trajectories. MD trajectories were analyzed using the ptraj module of AMBER 11. Various types of analyses consisting of calculation of the backbone root-mean-square deviation (rmsd), distances between functionally important residues, correlated dynamic motions, principal component analysis (PCA), and estimation of flexibilities of different segments in terms of root-mean-square fluctuation (rmsf) values were conducted. Structural superpositions were conducted using a local version of ProFit. Positional correlation plots were visualized using the pheatmap module of R (http://www.r-project.org).

Clustering of Conformers from MD Trajectories. To analyze the extent of conformational sampling and to compare conformers obtained from AMBER simulations with those from GROMACS, snapshots saved at an interval of 200 ps from the 1 μs AMBER and 100 ns GROMACS trajectories were clustered together. Thus, a total of 5500 intermediates from each of the MD simulations on monomer_S and monomer_E were separately subjected to k-mean clustering using the kclust utility in the MMTSB (Multiscale Modeling Tools for Structural Biology) suite.[29] The clustering was conducted on the basis of the Cα rmsd, and the clustering radius was set to 1.5 Å. This resulted in 31 clusters for intermediates from monomer_E simulations, while those from the monomer_S simulation constituted 32 clusters. To obtain a representative set of structures for the purpose of visualization, representative structures corresponding to centroids of each of these clusters were clustered again using a Cα rmsd clustering radius of 2 Å. This resulted in eight clusters for the monomer_E simulation and seven for monomer_S. In addition, the extent of conformational sampling in our monomer and dimer simulations was also assessed in terms of movement of the activation loop toward or away from the catalytic center by monitoring the distances between Ser/Thr on the activation loop and the closest Oδ atom of catalytic Asp138.

RESULTS

MD Simulations Reveal the Differential Dynamic Behavior of PknB in Monomeric and Dimeric States. To analyze the overall conformational changes in monomeric and dimeric PknB during 1 μs explicit solvent molecular dynamics simulations, the backbone rmsds with respect to the initial structures were analyzed over the entire 1 μs trajectory. Figure 2 shows rmsds excluding the activation loop region for both chains of the dimer as well as the phosphorylated (monomer_S) and nonphosphorylated monomer (monomer_S), while Figure S4A of the Supporting Information shows rmsds over the entire structures. The rmsd plots (Figure 2 and Figure S4A of the Supporting Information) for the monomer and dimer simulations over the entire 1 μs trajectory clearly demonstrate the convergence of all the simulations. Because the loop regions show higher flexibilities, exclusion of loop residues reduces rmsd values by ~1 Å for all structures. Monomer_E that contains phosphothreonine at position 171 shows an rmsd of ~2.5−3 Å over the entire 1 μs trajectory, while monomer_S that lacks phosphothreonine shows an rmsd of ~4−4.5 Å. This suggests that in the monomeric state of PknB, the enzymelike phosphorylated form is less flexible and more stable than the substratelike nonphosphorylated form. In contrast to the stabilizing effect of phosphorylation in the

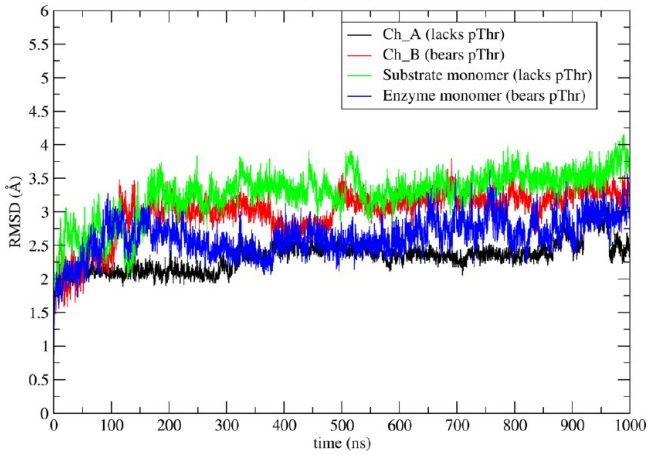

Figure 2. Backbone rmsd plots obtained after excluding the activation loop residues for each of the systems simulated [phosphorylated and nonphosphorylated chains of the dimer (dimer_E and dimer_S, respectively), enzymelike monomer phosphorylated on Thr171 (monomer_E), and nonphosphorylated substratelike monomer (monomer_S)].

monomeric state of PknB, surprisingly our simulations for the front-to-front dimeric state of PknB show a reverse trend. As can be seen, backbone rmsds of dimer_E and monomer_S are comparable (2.5−3.5 Å). Similarly, backbone rmsds of dimer_S and monomer_E are comparable to each other (~4 Å) (Figure S4A of the Supporting Information). To understand the origin of this differential dynamic behavior of the monomeric and dimeric states of PknB, we calculated the rmsds for each of the residues by superposing initial and final structures obtained after 1 μs simulations for monomer_E, monomer_S, and dimer (Figure S4B of the Supporting Information). Figure S5 of the Supporting Information shows computed rmsf values for various residues of monomeric and dimeric PknB. These results (Figures S4 and S5 of the Supporting Information) indicate that the higher rmsd in monomer_S essentially arises from the movement of the activation loop, while in phosphorylated monomer_E, the activation loop shows significantly less deviation. The higher rmsd in dimer_E arises from the movement of the activation loop and N-terminal domain. On the other hand, dimer_S shows a lower rmsd for both the activation loop and the N-terminal domain. This may be due to the restricted motions of the activation loop in the nonphosphorylated chain upon PknB dimerization. In fact, visual analysis of the relative orientations of activation loops of both chains of dimeric PknB (Figure 1) also reveals that the activation loop of the phosphorylated chain (dimer_E) is exposed to the solvent while the activation loop of the nonphosphorylated chain (dimer_S) is constrained within the catalytic cleft of the phosphorylated chain of the dimer.

Earlier structural studies[8,30] of kinase catalytic domains have highlighted the crucial role of some of the key subfragments in the inactive to active conformational transition of kinases. For example, movement of helix αC controls the relative orientation of N- and C-terminal lobes. The orientation of the Mg^{2+}-binding loop controls ATP binding. In the active form of kinases, the activation loop remains away from the catalytic pocket, while in catalytically inactive forms, the activation loop is known to move toward the catalytic pocket, thus obstructing binding of substrate peptides. Similarly, intermolecular contacts involving helix G are known to control the oligomerization

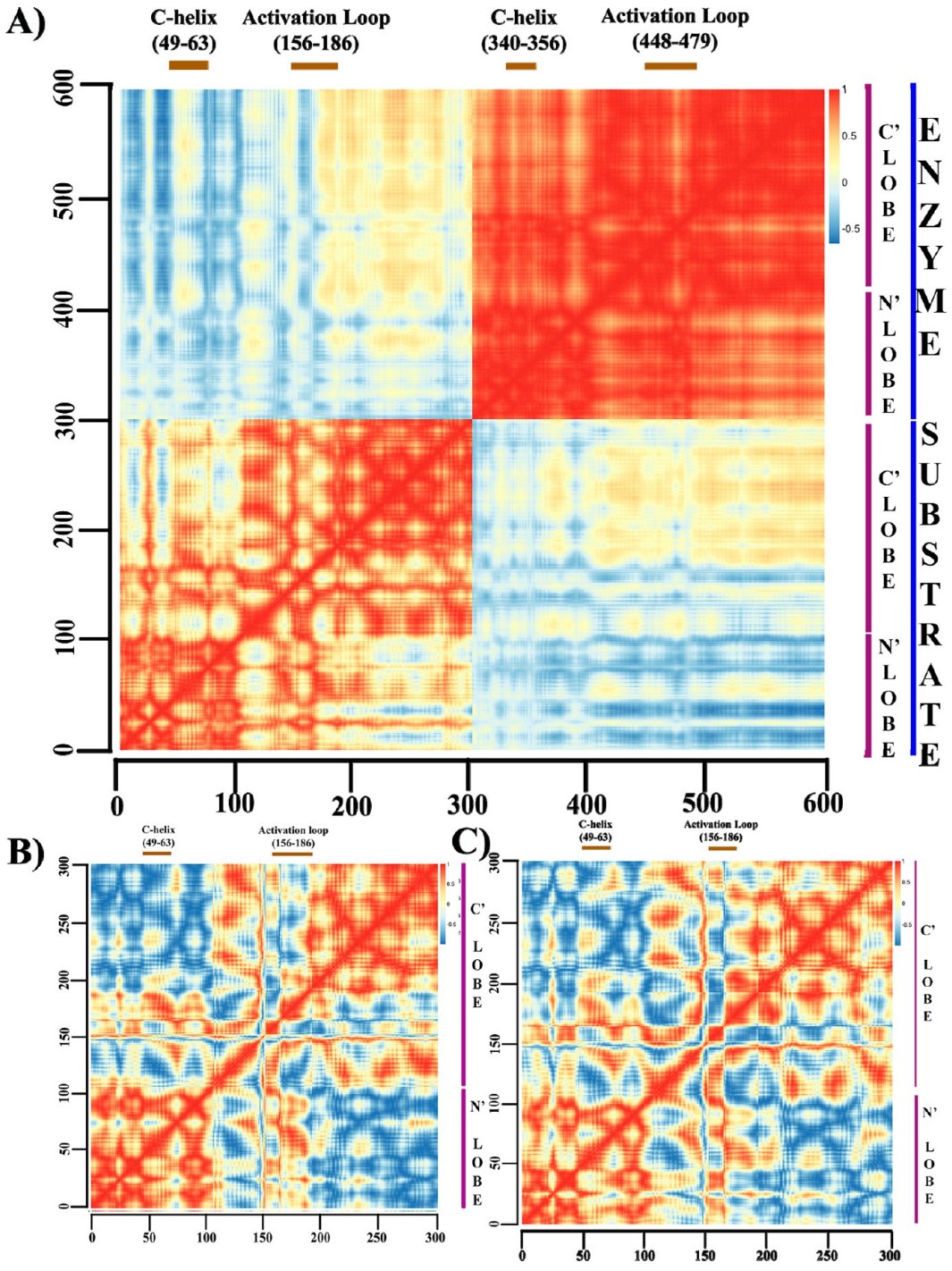

Figure 3. Residuewise correlation plots of (A) the dimer, (B) the substrate monomer, and (C) the enzyme monomer calculated over the entire 1 μs. N- and C-lobes as well as individual structural subfragments are labeled on every panel to highlight the correlated motions between them. Correlations are stronger in dimer than in monomeric forms.

status of kinases, and hence, it can play a crucial role in trans autophosphorylation.[6] Therefore, we also investigated the effect of phosphorylation on the flexibilities of various structural subfragments of PknB by computing rmsf values for helix αC, the Mg^{2+}-binding loop, the activation loop, and helix G in phosphorylated and nonphosphorylated PknB in monomeric and dimeric states. The most pronounced effect of phosphorylation is observed on the Mg^{2+}-binding loop, which shows reduced fluctuations, both in monomers and in the dimer, thereby optimally positioning Phe157 to form a well-assembled R spine.[31]

To explore the correlations between movements of various structural subfragments, we analyzed the average cross correlation between displacement of different residues of the dimer, monomer_S, and monomer_E over the 1 μs trajectory by calculating the mass-weighted residue correlation matrix (Figure 3). In the trajectories for both monomeric forms of PknB, there is a positive correlation between movements of the smaller N-terminal lobe and those of the larger C-terminal lobe.

dx.doi.org/10.1021/bi500245v | *Biochemistry* 2014, 53, 4715−4726

Interestingly, compared to the monomers, the interlobe movement becomes significantly more correlated in enzymelike phosphorylated chain B of dimeric PknB, while the interlobe movement is less correlated in substratelike chain A (Figure 3A). This indicates that movement of the N-lobe with respect to the C-lobe is more pronounced in substratelike chain A of the dimer. Thus, our simulations suggest that front-to-front dimerization can indeed enhance the extent of interlobe movement in each of its chains.

Analysis of Conserved Residue Interaction Networks. Relative movements of the two lobes of the kinase catalytic domain drive the process of activation in many kinases.[30] Therefore, we intended to investigate the alterations in inter-residue contact networks in PknB resulting from movement of its smaller N-lobe with respect to the larger C-lobe. The K72−E91 (numbering of the PKA structure of PDB entry 1JBP) interaction is a conserved salt bridge interaction that is a hallmark of several active state eukaryotic protein kinases (EPKs) and eukaryotic-like kinases (ELKs).[30] This salt bridge is often disrupted in the inactive state conformations because the Lys residue cannot orient β- and γ-phosphates of ATP for optimal phosphate transfer. Therefore, we monitored the electrostatic interaction between corresponding residues Lys40 and Glu59 in PknB and measured the distances between the Nζ atom of Lys40 and the closest Oε atom of Glu59 over 1 μs by extracting intermediate structures at regular intervals of 200 ps. Interestingly, we observed that this salt bridge interaction is preserved in phosphorylated forms of PknB (monomer_E and dimer_E) (Figure 4). In nonphosphorylated monomer_S, this salt bridge was observed to be broken and formed several times over the 1 μs trajectory, indicating a transition between the inactive and active state. However, in nonphosphorylated chain A of the dimer (dimer_S), after the first 50 ns this salt bridge was essentially broken and the K40−E59 pair remained mostly at a distance of 8−9 Å during the rest of the 1 μs trajectory (Figure 4). These results indicate that the pronounced interdomain movement seen in the nonphosphorylated chain of the dimer (dimer_S) indeed corresponds to a transition from an active to an inactive-like conformation in terms of interlobe orientation.

Similarly, two hydrophobic spines are known to stabilize the EPK catalytic domains.[31] These spines are assembled only in the active state conformations of kinases. We identified residues Ala63, Val74, His136, and Phe157, which constitute the regulatory R spine in PknB based on the structure-guided multiple-sequence alignment of PknB with two other eukaryotic prototype kinases, namely, PKA and CDK2 (Figure S6 of the Supporting Information) in PROMALS3D.[32] As shown in Figure 5, the distance between the Ala63 and Phe157 pair is likely to be maximally affected by interlobe movement. Hence, we monitored the hydrophobic packing of these residues in monomeric forms over 1 μs. It was observed that the R spine was disrupted in the PknB substrate monomer (Figure 5B) because of the increase in the distance between Ala63 and Phe157. However, the R spine in the enzyme monomer was found to be intact throughout the 1 μs simulation (Figure 5C). Figure S7 of the Supporting Information shows the corresponding R spine analysis for the two chains of the dimer over the 1 μs trajectory. Thus, analysis of the R spine also correlates with earlier results that suggest interlobe movement in monomer_S as well as the non-phosphorylated chain of the dimer toward the inactive conformation. In contrast to the R spine, the hydrophobic

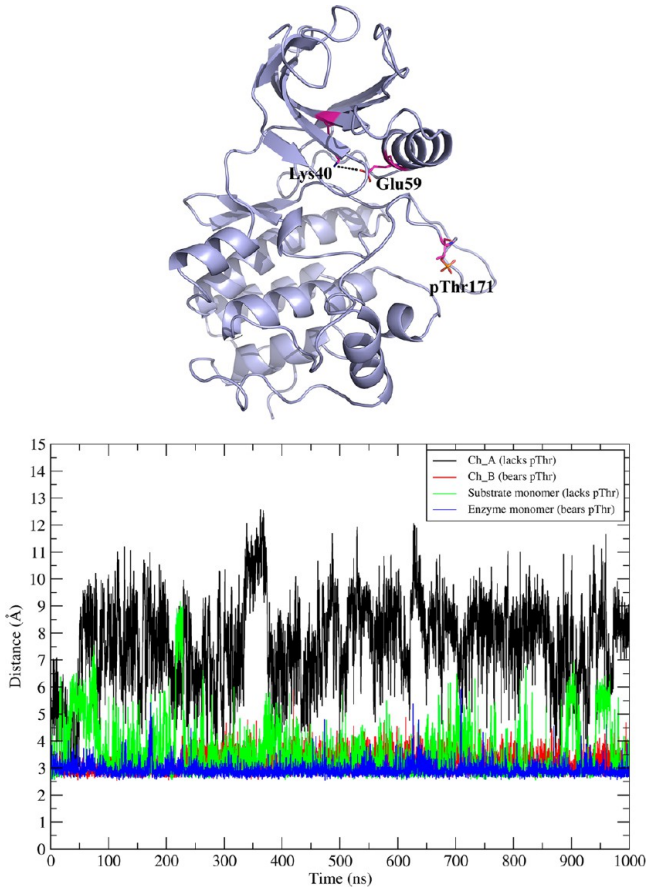

Figure 4. Cartoon representation of the PknB catalytic domain (top) with interactions between Lys40 and Glu59 depicted, an electrostatic interaction characteristic of active state kinase structures. The distance between the Nζ atom of Lys40 and the closest Oε atom of Glu59 is plotted vs simulation time (bottom). This salt bridge is maintained within 4 Å only in phosphorylated forms of PknB. Thus, phosphorylation stabilizes the PknB catalytic domain in the activelike conformational state: black for the nonphosphorylated chain of the dimer, red for the phosphorylated chain of the dimer, green for the substrate monomer, and blue for the enzyme monomer.

interactions between residues constituting the catalytic C spine did not show stark differences in phosphorylated and nonphosphorylated forms of PknB.

Intermolecular Trans Autophosphorylation in the PknB Dimer. PknB is known to be activated through autophosphorylation of one or more of the Ser/Thr residues on its activation loop. Thr171 and Thr173 are known to be the major primary and secondary autophosphorylation, sites respectively, though others like Ser169 and Thr179 have also been found to be phosphorylated in different experimental setups.[6] Trans autophosphorylation in the front-to-front dimer is intuitive, and it has been proposed that the activation loop of the nonphosphorylated chain moves into the active site of the phosphorylated chain. Therefore, we first investigated the feasibility of trans autophosphorylation in the front-to-front dimer of PknB as proposed by Mieczowski et al.[6] However, in the static crystal structure of the front-to-front dimer of PknB, these potential autophosphorylation sites on the nonphosphorylated chain are located far from the catalytic pocket of the phosphorylated chain. Distances between the Oγ atom of Ser/Thr on the activation loop of the nonphosphorylated chain and the closest Oδ atom of the catalytic Asp138 of the

dx.doi.org/10.1021/bi500245v | Biochemistry 2014, 53, 4715−4726

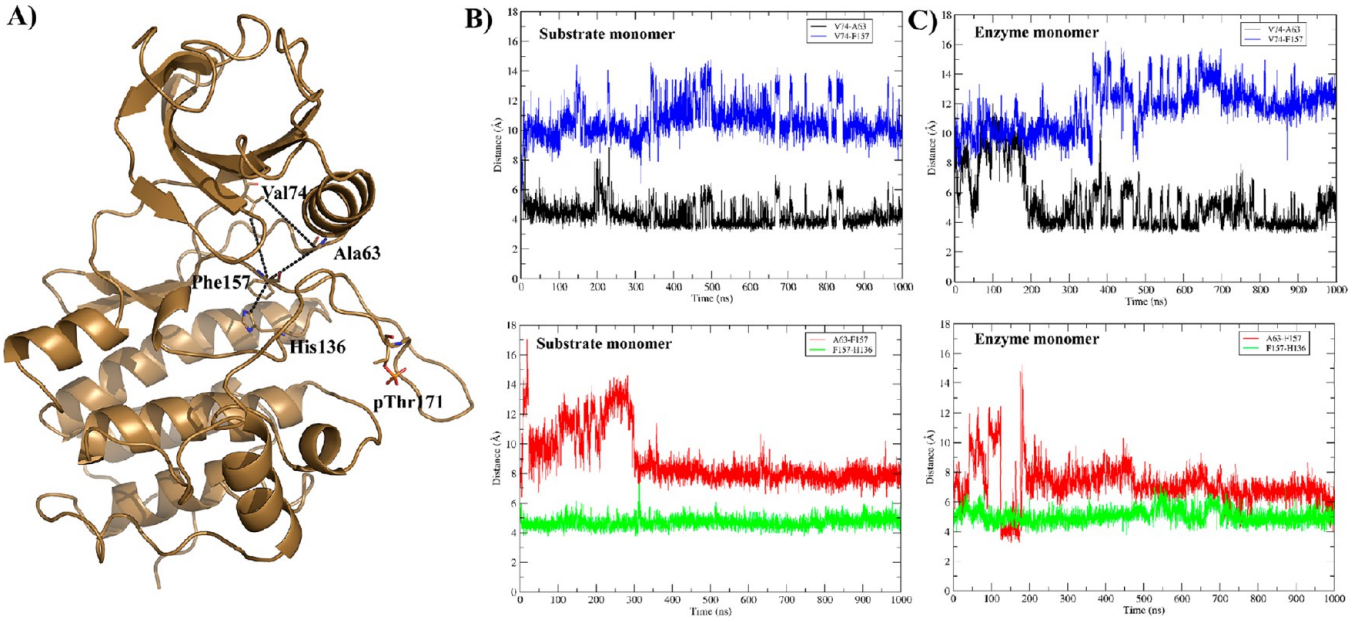

Figure 5. (A) Residues constituting the R spine are depicted on the structure of the phosphorylated monomer of PknB. Distances between the closest atoms of these residues are plotted vs time in (B) the substrate monomer and (C) enzyme monomers. The distances between A63 and V74 and between V74 and F157 are separated from the distances between A63 and F157 and between F157 and H136 for the sake of clarity.

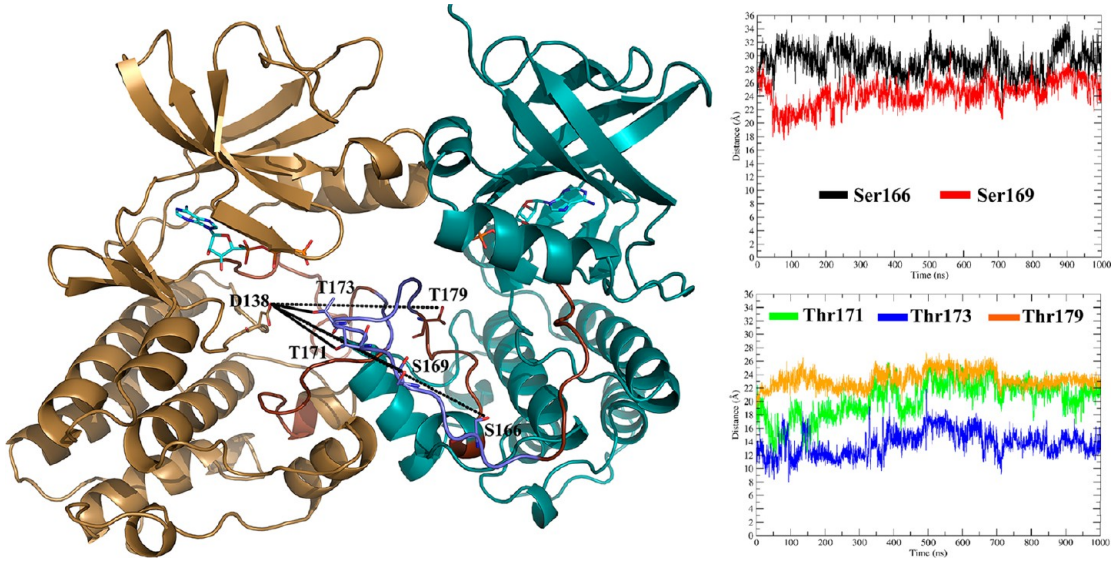

Figure 6. (A) Distances between Ser/Thr residues on the activation loop of the substratelike nonphosphorylated chain (teal) and the catalytic Asp138 on the enzymelike phosphorylated chain (gold) are depicted on the PknB dimeric structure. (B) Distances between the Oγ atom of Ser/Thr residues on the activation loop of the nonphosphorylated chain and the closest Oδ atom of the catalytic Asp138 on the phosphorylated chain of the dimer are plotted vs time: black for Ser166, red for Ser169, green for Thr171, blue for Thr173, and orange for Thr179. Ser-Asp pairs have been separated from Thr-Asp pairs for the sake of clarity.

phosphorylated chain fall in the range of 13−30 Å. Thus, the phosphate transfer seems to be geometrically infeasible in the static crystal structure. We wanted to investigate if explicit solvent MD simulations for 1 μs can induce movement of the activation loop of the nonphosphorylated chain toward the catalytic Asp of the phosphorylated chain. The distances between each of these five potential autophosphorylation sites on the activation loop of the nonphosphorylated chain in the dimer from the catalytic Asp138 of the phosphorylated chain were computed over 1 μs of the MD trajectory (Figure 6), and their distributions were analyzed (Figure S8 of the Supporting Information). Surprisingly, of the five phosphorylatable residues on the nonphosphorylated chain (dimer_S), only Thr173, which was initially at a distance of 13.26 Å, moves slightly closer to the active site pocket of the phosphorylated chain (dimer_E) and remains 10−12.5 Å from the catalytic Asp138 of dimer_E during the major part (~350 ns) of the 1 μs simulation (Figure 6). On the other hand, all other phosphorylatable residues remain at distances ranging from 17 to 30 Å throughout the 1 μs trajectory. It should be noted here that the entry of the activation loop of the nonphosphorylated chain (dimer_S) into the active site pocket of the phosphorylated chain (dimer_E) is a concerted effect of the surrounding Ser/Thr residues on its own activation loop as well

dx.doi.org/10.1021/bi500245v | *Biochemistry* 2014, 53, 4715−4726

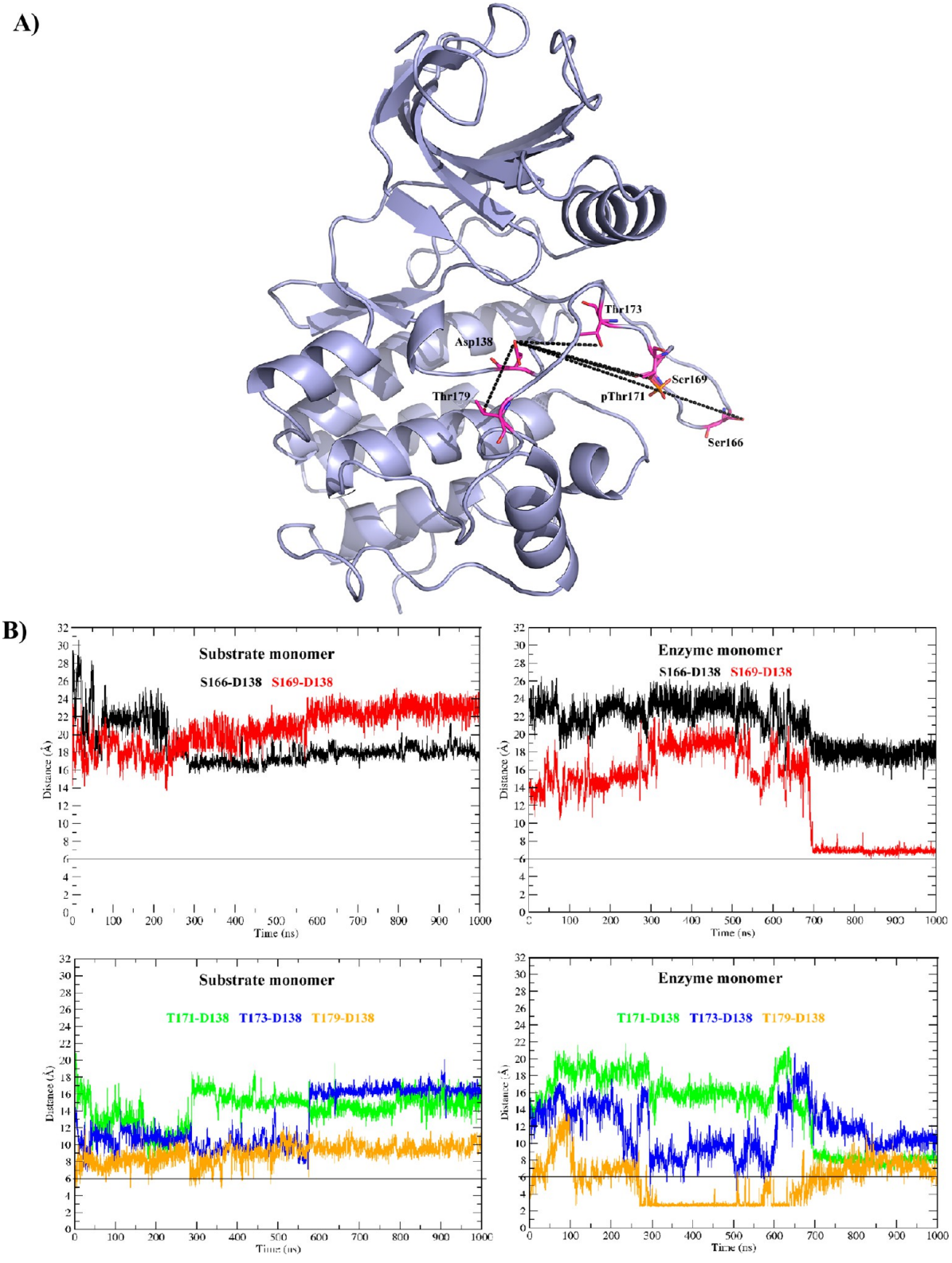

Figure 7. (A) Distances between Ser/Thr residues on the activation loop and the catalytic Asp138 within the same monomer have been depicted on the phosphorylated monomer of PknB. (B) Distances between the Oγ atom of Ser/Thr residues on the activation loop and the closest Oδ atom of the catalytic Asp138 in the monomeric forms of PknB are plotted vs time in the substrate (left) and enzyme monomer (right): black for Ser166, red for Ser169, green for Thr171, blue for Thr173, and orange for Thr179.

as the activation loop of the phosphorylated chain. Therefore, the electrostatic interactions between the activation loop residues of the nonphosphorylated chain and the spatial constraints from the activation loop of the phosphorylated chain are crucial factors regulating this movement. It is also possible that conformational changes required for trans autophosphorylation could not be sampled even during the 1 μs simulation of dimeric PknB.

dx.doi.org/10.1021/bi500245v | *Biochemistry* 2014, 53, 4715−4726

Mechanistic Details of Novel Cis Autophosphorylation Unraveled by MD Simulations. Because our simulations of monomer_S and monomer_E had revealed significant movements of the activation loop during the 1 μs explicit solvent simulation, we also investigated the geometric feasibility of cis autophosphorylation in which one monomer would phosphorylate the Ser/Thr residues on its own activation loop. The distance between the Oγ atom of these Ser/Thr residues and the closest Oδ atom of the catalytic Asp138 on the same monomer was analyzed in the MD trajectories of monomer_S and monomer_E (Figures 7B,C), and the distributions of these distances are shown in Figure S9 of the Supporting Information. In the starting crystal structure for monomer_S, the Thr179 was ~10 Å from the catalytic Asp138, while four other phosphorylatable residues were more than 12 Å from the catalytic Asp138. During the 1 μs simulation, Ser166 and Ser169 remain away from the catalytic Asp138 at distances >17 Å, but Thr179, Thr173, and Thr171 move significantly closer to the catalytic Asp138. As shown in Figure 7B, Thr179 approaches catalytic Asp138 with a distance of 5−6 Å at several points during the simulation and remains at an average distance of 8 Å for almost 600 ns. Similarly, Thr171 and Thr173, which were >12−15 Å from the catalytic center in the initial structure, moved to a distance of 9−10 Å at ~200 ns. During the 200−300 ns period, Thr171 remained at a distance of approximately 10 Å. Similarly, Thr173 remained ~9 Å from Asp138 during the 300−600 ns period, but Thr171 moved away. Thus, our simulations of the substratelike monomer of PknB revealed the movement of the activation loop into its own catalytic pocket, and these results suggest the interesting possibility of cis autophosphorylation within the same monomer. Detailed analysis of the snapshots from these trajectories revealed that, even though Thr179 can move within 6−7 Å of the catalytic Asp138, it remained away from the γ-phosphate of ATP at distances of ~12 Å (Figure S10 of the Supporting Information). On the other hand, Thr173 remained ~7.5 Å from Asp138, but the γ-phosphate of ATP came within 3.5 Å (Figure S10 of the Supporting Information). Similarly, at an earlier time point in the trajectory, we observed Thr171 approaching the catalytic Asp138 at a distance of 8.5 Å. The distance of the γ-phosphate of ATP from Thr171 in this snapshot was 3.6 Å. Because phospho-transfer requires proximity to both ATP and Asp138, it is possible that some of these conformations for monomer_S sampled during our MD simulations might indeed facilitate cis autophosphorylation of Thr171 and Thr173. Interestingly, Thr171 and Thr173 are indeed the experimentally identified primary and secondary autophosphorylation sites, respectively, for PknB.[12] Thus, our simulations also provide a structural basis for the preferential autophosphorylation of Thr171 and Thr173 from among the five phosphorylatable residues in the activation loop of PknB. These MD simulations reveal the novel possibility of cis autophosphorylation in PknB monomers. Even though trans autophosphorylation via formation of the front-to-front dimer is the currently accepted model for autophosphorylation of PknB, results from our simulations on monomeric PknB have interesting biological implications because of the availability of the crystal structure of PknB in the back-to-back dimeric form. In the back-to-back dimeric state, active sites of the two monomers face opposite each other; hence, cis autophsophorylation within each monomer could indeed be an alternate mode of autophosphorylation.

Effect of Prior Phosphorylation on Movements of the Activation Loop. We also analyzed the movement of the activation loop in the MD trajectories of monomer_E, which is phosphorylated at the primary autophosphorylation site Thr171 (Figure S10C of the Supporting Information). It is interesting to note that, in contrast to monomer_S simulations in which Thr171 moves toward the catalytic Asp138, in monomer_E simulations phospho-Thr171 remained consistently away from the Asp138 at distances of >15 Å for almost 700 ns. However, in the monomer_E simulations, Thr173 remained 5−8 Å from the catalytic Asp138 for 300 ns, and its orientation with respect to the γ-phosphate of ATP can potentially facilitate phospho-transfer (Figure S10C of the Supporting Information). In the monomer_E simulations, Thr179 also remained ~4 Å from Asp138 for ~400 ns, but it remained away from the γ-phosphate of ATP. Thus, our simulations reveal that phosphorylation on primary autophosphorylation site Thr171 systematically guides the movement of other Ser/Thr residues on the activation loop toward its own active site pocket. Moreover, the movements of Thr173 and Thr179 are negatively correlated. Thus, Thr173 and Thr179 both approach the catalytic Asp138 alternately. Thus, these MD studies reveal the novel possibility of cis autophosphorylation in PknB monomers and suggest phosphorylation of secondary autophosphorylation site Thr173 in a cooperative manner in the presence of prior phosphorylation on primary autophosphorylation site Thr171.

Comparison between AMBER and GROMACS Simulations and Analyses of the Extent of Conformational Sampling. We wanted to compare if results on the dynamic behavior of PknB obtained from AMBER simulations can be reproduced with GROMACS, which uses a different force field. However, GROMACS simulations were conducted for 100 ns only, as similar trends in results were observed for the dimer and monomers, as well. For equivalent pairs of systems, the first 100 ns of the 1 μs AMBER MD trajectory was compared with the 100 ns trajectory from GROMACS. The backbone rmsd from the initial structure and movement of the activation loop as measured by the distance from phosphorylatable Ser/Thr residues to the catalytic Asp were compared. Both phosphorylated (monomer_E) and nonphosphorylated (monomer_S) monomers show very similar rmsd values (Figure S11 of the Supporting Information). Similarly, the phosphorylated chain of the dimer (dimer_E) shows similar rmsd values in both AMBER and GROMACS trajectories, while the nonphosphorylated chain of the dimer (dimer_S) shows significant differences in rmsds (Figure S11 of the Supporting Information). Analysis of rmsds for individual components as well as visual analysis of the trajectories revealed that the modeled activation loop of dimer_S remained closer to the initial conformation in the AMBER simulation while in the GROMACS simulations, it moved away from its modeled conformation toward the active site of the other monomer. A comparison of distances between potential phospho-sites on the activation loop and catalytic Asp138 (Figure S12 of the Supporting Information) over the AMBER and GROMACS trajectories also revealed a similar trend. In the case of the dimer, the Ser/Thr residues of the nonphosphorylated chain are closer to Asp138 of the phosphorylated chain in the GROMACS trajectory than in the AMBER trajectory. However, for the monomers, some of the conformers visited during 100 ns of the GROMACS trajectory were also visited at a later time point during the 1 μs of the AMBER trajectory.

dx.doi.org/10.1021/bi500245v | *Biochemistry* 2014, 53, 4715−4726

We also analyzed the GROMACS simulation results in detail to understand the effect of phosphorylation on the Lys40−Glu59 salt bridge (Figure S13 of the Supporting Information) and the residue network forming the R spine (Figure S14 of the Supporting Information). Interestingly, the results in Figures S13 and S14 of the Supporting Information from the 100 ns GROMACS simulation are very similar to corresponding results from AMBER simulations shown in Figures 4 and 5, respectively. During our 100 ns MD simulations on the dimer in GROMACS, Thr171 and Thr173 for most of the simulation (i.e., approximately 70 of 100 ns) remained 10 and 7.5 Å, respectively, from the catalytic Asp138 of the phosphorylated chain (Figure S15 of the Supporting Information). Similarly, during the 100 ns GROMACS simulation on the non-phosphorylated monomer (monomer_S), Thr171 and Thr173 moved within 9 Å of the catalytic Asp from their initial positions, which were beyond 12−15 Å (Figure S16 of the Supporting Information). Thus, similar to the results from the AMBER simulation (Figure 7), the GROMACS simulation (Figure S16 of the Supporting Information) on the non-phosphorylated monomer also shows folding of the activation loop toward the catalytic pocket. These results indicated that comparable dynamics is reproduced for PknB even by simulations with two different force fields.

Because both our AMBER and GROMACS simulations revealed an interesting possibility of folding of the activation loop of the nonphosphorylated monomer into its own active site pocket, we also analyzed the extent of conformational sampling of this loop region during our monomer simulations. As mentioned in Materials and Methods, clustering of 5500 conformers from 100 ns of GROMACS and 1 μs of AMBER trajectories for equivalent pairs of systems resulted in 32 clusters for monomer_S and 31 clusters for monomer_E at a clustering radius of 1.5 Å (Figure S17 of the Supporting Information). This clearly suggests many of the structures have been visited multiple times during our MD simulations, thus indicating adequate conformational sampling and convergence of simulations. To reduce the number of representative structures for the sake clarity in visualization, the structures corresponding to centroids of each of the clusters mentioned above were clustered again using a Cα rmsd clustering radius of 2 Å. This resulted in eight clusters for the monomer_E simulation and seven for monomer_S. It is important to note that the clustering radius refers to the rmsd over the entire structure, while the rmsd over the loop region for a pair of representative structures will be significantly higher. Figure 8 shows the superposition of these eight structures for monomer_E and seven structures for monomer_S over their respective starting structures. As one can see (Figure 8), activation loop regions have been adequately sampled and have moved significantly away from their starting positions.

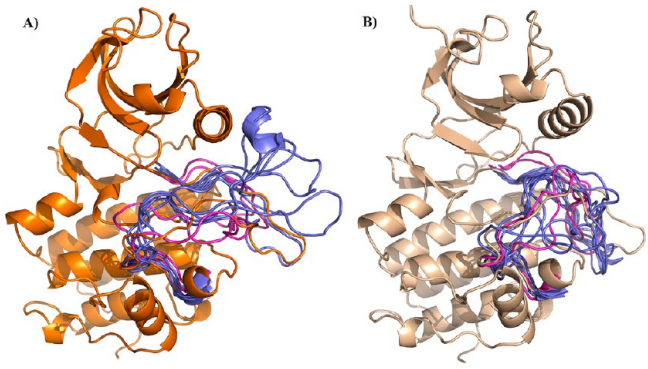

Figure 8. Clustering of conformations sampled during MD simulations on (A) monomer_S and (B) monomer_E. Representative structures corresponding to centroids of sampled clusters have been superposed on their respective initial structures (monomer_S colored orange and monomer_E colored light orange). Activation loop orientations visited during 1 μs MD simulations in AMBER on monomer_S and monomer_E are colored blue, while those visited during 100 ns MD simulations in GROMACS are colored magenta. Relative orientations of N- and C-terminal lobes did not show any major alterations and, therefore, have been omitted from the cartoon representation for the sake of clarity.

DISCUSSION

Atomistic simulations have been extensively used to explore the conformational transitions between inactive and active states of several eukaryotic kinases such as Abl, Src, Syk, CDK5, and PKA.[33−38] However, to the best of our knowledge, the conformational transition associated with autophosphorylation of kinases has not been explored by atomistic simulations. Similarly, no simulation studies have attempted to explore how exactly prior phosphorylation of activation loop residues drives inactive to active state conformational transitions in kinases. Because the autophosphorylation process requires an inactive kinase molecule to adopt an active conformation and phosphorylate its own activation loop, mechanistic details of autophosphorylation have posed several intriguing questions. On the basis of the front-to-front dimer crystal structure and other biochemical experiments, the intermolecular trans autophosphorylation model has been proposed, and it is a widely accepted mechanism of autophosphorylation for several kinases, including mycobacterial PknB. However, atomistic details of intermolecular autophosphorylation are not always apparent because of the disordered activation loops in many of these crystal structures. Second, the availability of back-to-back dimeric structures for PknB also suggests the possibility of intramolecular cis autophosphorylation. Therefore, in this work, we have performed a series of 1 μs atomically detailed explicit solvent molecular dynamics simulations on phosphorylated and nonphosphorylated states of monomeric and dimeric PknB catalytic domains to explore the conformational transitions associated with autophosphorylation.

Our simulations reveal that phosphorylation on Thr171 alters the relative orientation of the smaller N-terminal lobe with respect to the larger C-terminal lobe of PknB. This involves the establishment and maintenance of crucial electrostatic and hydrophobic interactions. The Lys−Glu salt bridge that is a hallmark interaction of active state conformations in eukaryotic kinases remains intact only in the presence of prior phosphorylation on the activation loop. Similarly, the hydrophobic regulatory R spine is well-assembled only in phosphorylated forms, thereby positioning helix αC in its active state conformation. Thus, phosphorylation stabilizes the active enzymelike state of PknB, while the nonphosphorylated forms resemble more inactive-like or substratelike conformations.

Our simulation studies have also explored the conformational transitions associated with the two alternate modes of autophosphorylation. Even though intermolecular trans autophosphorylation involving formation of the front-to-front dimer is most intuitive, in the initial starting structures of the PknB front-to-front dimer, the secondary autophosphorylation site Thr173 on the activation loop of the substratelike chain was

situated 7.2 Å from the γ-phosphate of ATP and 9.6 Å from the catalytic Asp138 of the enzymelike chain. In our 1 μs simulations of dimeric PknB, the corresponding distance between Thr173 on the substratelike chain and catalytic Asp138 of the enzymelike chain remained in the range of 9−15 Å. It is possible that even if our simulation of dimeric PknB covers 1 μs, it has not been able to sample the required conformational changes for trans autophosphorylation. On the other hand, in our simulations of nonphosphorylated monomeric PknB, the activation loop was observed to fold into its own active site, moving within approximately 5−6 Å of the catalytic Asp138. In fact, primary and secondary autophosphorylation sites Thr171 and Thr173 move within 3.5 and 3.6 Å, respectively, of the γ-phosphate of ATP. Our simulations also reveal that phosphorylation on primary autophosphorylation site Thr171 systematically guides the movement of other Ser/Thr residues on the activation loop toward its own active site pocket. Thus, our monomer simulations demonstrate the conformational feasibility of intramolecular cis autophosphorylation for PknB.

Also, our results suggest that autophosphorylation of inactive monomers of PknB might be initiated through the intramolecular cis mechanism. Once phosphorylated, the activation loop flips away from the catalytic pocket and the monomer becomes fully active for the subsequent trans autophosphorylation or phosphorylation of other downstream substrate proteins (Figure 9). *In vitro* kinase assays can be performed to test this hypothesis using the PknB catalytic domain harboring suitably designed mutations on the dimerization interface that would eliminate the possibilities of both back-to-back and front-to-front dimerization. The ability of cis autophosphorylation can be tested by comparing activities of these interface mutants in the presence of [γ-^{32}P]ATP with purified forms of wild-type PknB. Detection of phosphorylation on an autoradiogram would indicate the cis mode of autophosphorylation. On the other hand, autophosphorylation in the trans mode can be tested using wild-type His-tagged PknB and GST or MBP-tagged K40M mutant PknB. Lys40, as discussed above, is crucial for the successful phospho-transfer as it helps in the proper orientation of the β- and γ-phosphates of ATP. The K40M mutation would, thus, make PknB inactive and catalytically incompetent with respect to bringing about phospho-transfer. Detection of phosphorylation on the kinase dead K40M PknB mutant in the presence of wild-type His-PknB or its dimerization interface mutants would indicate the ability of PknB to trans phosphorylate. Apart from these site-directed mutagenesis-based experiments, analysis of the reaction kinetics of phosphorylation by PknB could also provide evidence of intramolecular cis autophosphorylation proposed by our simulations. Comparison of rates of substrate phosphorylation by wild-type PknB and PknB co-expressed with its cognate phosphatase PstP in *M. tuberculosis* can shed light on differential reaction kinetics of cis and trans modes of autophosphorylation. Interestingly, on the basis of similar reaction kinetics studies, recently the cis autophosphorylation mechanism has been proposed for other eukaryotic kinases like PAK2, Chk2, and Aurora-A.[16,17] Therefore, we believe our simulation results will prompt the experimental community to test the proposed cis autophosphorylation mechanism for PknB.

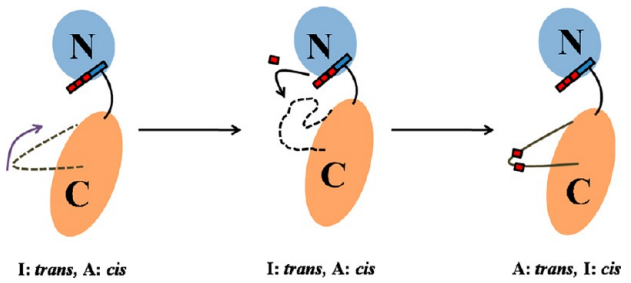

Figure 9. Schematic representation of the possible activation of the PknB monomer through cis autophosphorylation. N- and C-terminal lobes are colored blue and orange, respectively, and labeled accordingly. In the unphosphorylated monomer (left), the activation loop shows a tendency to refold (arrow pointing inward) into the catalytic pocket of the same monomer, rendering it active for cis autophosphorylation. However, this monomer is inactive for trans autophosphorylation because of a lack of phosphate on the activation loop. Once the activation loop refolds into the catalytic pocket, it might become phosphorylated by the same monomer in the cis mode (center) and, once phosphorylated, flip away from the pocket (right) so that it is fully active for subsequent trans autophosphorylation and phosphorylation of other downstream substrate proteins.

■ ASSOCIATED CONTENT

Supporting Information

Figures S1−S17 described in the text. This material is available free of charge via the Internet at http://pubs.acs.org.

■ AUTHOR INFORMATION

Corresponding Author

*Bioinformatics Center, National Institute of Immunology, Aruna Asaf Ali Marg, New Delhi 110067, India. E-mail: deb@nii.res.in. Telephone: +91-11-26703749.

Funding

This work was supported by the Department of Biotechnology (DBT), Government of India, a grant to the National Institute of Immunology, New Delhi, grants to D.M. from DBT, India. under the BTIS project, and a National Bioscience Career Development award. N.P.D. is grateful to DBT, India, for the BINC fellowship.

Notes

The authors declare no competing financial interest.

■ ACKNOWLEDGMENTS

We acknowledge help from Dr. Vinay Nandicoori in critical reading of the manuscript and valuable discussions.

■ REFERENCES

(1) Fernandez, P., Saint-Joanis, B., Barilone, N., Jackson, M., Gicquel, B., Cole, S. T., and Alzari, P. M. (2006) The Ser/Thr protein kinase PknB is essential for sustaining mycobacterial growth. *J. Bacteriol. 188*, 7778−7784.

(2) Sassetti, C. M., Boyd, D. H., and Rubin, E. J. (2003) Genes required for mycobacterial growth defined by high density mutagenesis. *Mol. Microbiol. 48*, 77−84.

(3) Mir, M., Asong, J., Li, X., Cardot, J., Boons, G. J., and Husson, R. N. (2011) The extracytoplasmic domain of the *Mycobacterium tuberculosis* Ser/Thr kinase PknB binds specific muropeptides and is required for PknB localization. *PLoS Pathog. 7*, e1002182.

(4) Barthe, P., Mukamolova, G. V., Roumestand, C., and Cohen-Gonsaud, M. (2010) The structure of PknB extracellular PASTA domain from *Mycobacterium tuberculosis* suggests a ligand-dependent kinase activation. *Structure 18*, 606−615.

(5) Ortiz-Lombardia, M., Pompeo, F., Boitel, B., and Alzari, P. M. (2003) Crystal structure of the catalytic domain of the PknB serine/

threonine kinase from *Mycobacterium tuberculosis*. *J. Biol. Chem. 278*, 13094−13100.
(6) Mieczkowski, C., Iavarone, A. T., and Alber, T. (2008) Auto-activation mechanism of the *Mycobacterium tuberculosis* PknB receptor Ser/Thr kinase. *EMBO J. 27*, 3186−3197.
(7) Wehenkel, A., Fernandez, P., Bellinzoni, M., Catherinot, V., Barilone, N., Labesse, G., Jackson, M., and Alzari, P. M. (2006) The structure of PknB in complex with mitoxantrone, an ATP-competitive inhibitor, suggests a mode of protein kinase regulation in mycobacteria. *FEBS Lett. 580*, 3018−3022.
(8) Johnson, L. N., Noble, M. E., and Owen, D. J. (1996) Active and inactive protein kinases: Structural basis for regulation. *Cell 85*, 149−158.
(9) Boitel, B., Ortiz-Lombardia, M., Duran, R., Pompeo, F., Cole, S. T., Cervenansky, C., and Alzari, P. M. (2003) PknB kinase activity is regulated by phosphorylation in two Thr residues and dephosphorylation by PstP, the cognate phospho-Ser/Thr phosphatase, in *Mycobacterium tuberculosis*. *Mol. Microbiol. 49*, 1493−1508.
(10) Duran, R., Villarino, A., Bellinzoni, M., Wehenkel, A., Fernandez, P., Boitel, B., Cole, S. T., Alzari, P. M., and Cervenansky, C. (2005) Conserved autophosphorylation pattern in activation loops and juxtamembrane regions of *Mycobacterium tuberculosis* Ser/Thr protein kinases. *Biochem. Biophys. Res. Commun. 333*, 858−867.
(11) Young, T. A., Delagoutte, B., Endrizzi, J. A., Falick, A. M., and Alber, T. (2003) Structure of *Mycobacterium tuberculosis* PknB supports a universal activation mechanism for Ser/Thr protein kinases. *Nat. Struct. Biol. 10*, 168−174.
(12) Kang, C. M., Abbott, D. W., Park, S. T., Dascher, C. C., Cantley, L. C., and Husson, R. N. (2005) The *Mycobacterium tuberculosis* serine/threonine kinases PknA and PknB: Substrate identification and regulation of cell shape. *Genes Dev. 19*, 1692−1704.
(13) Lombana, T. N., Echols, N., Good, M. C., Thomsen, N. D., Ng, H. L., Greenstein, A. E., Falick, A. M., King, D. S., and Alber, T. (2010) Allosteric activation mechanism of the *Mycobacterium tuberculosis* receptor Ser/Thr protein kinase, PknB. *Structure 18*, 1667−1677.
(14) Yeats, C., Finn, R. D., and Bateman, A. (2002) The PASTA domain: A β-lactam-binding domain. *Trends Biochem. Sci. 27*, 438.
(15) Wang, J., Wu, J. W., and Wang, Z. X. (2011) Structural insights into the autoactivation mechanism of p21-activated protein kinase. *Structure 19*, 1752−1761.
(16) Wang, J., Wu, J. W., and Wang, Z. X. (2011) Mechanistic studies of the autoactivation of PAK2: A two-step model of cis initiation followed by trans amplification. *J. Biol. Chem. 286*, 2689−2695.
(17) Dodson, C. A., Yeoh, S., Haq, T., and Bayliss, R. (2013) A kinetic test characterizes kinase intramolecular and intermolecular autophosphorylation mechanisms. *Sci. Signaling 6*, ra54.
(18) Eswar, N., Webb, B., Marti-Renom, M. A., Madhusudhan, M. S., Eramian, D., Shen, M. Y., Pieper, U., and Sali, A. (2006) Comparative protein structure modeling using Modeller. *Current Protocols in Bioinformatics*, Chapter 5, Unit 5.6, p 130, Wiley, New York.
(19) Case, D. A., Darden, T., Cheatham, T. E., III, Simmerling, C. L., Wang, J., Duke, R. E., Luo, R., Walker, R. C., Zhang, W., Merz, K. M., Roberts, B., Wang, B., Hayik, S., Roitberg, A., Seabra, G., Kolossváry, I., Wong, K. F., Paesani, F., Vanicek, J., Liu, J., Wu, X., Brozell, S. R., Steinbrecher, T., Gohlke, H., Cai, Q., Ye, X., Wang, J., Hsieh, M.-J., Cui, G., Roe, D. R., Mathews, D. H., Seetin, M. G., Sagui, C., Babin, V., Luchko, T., Gusarov, S., Kovalenko, A., and Kollman, P. A. (2010) *AMBER 11*, University of California, San Francisco.
(20) Duan, Y., Wu, C., Chowdhury, S., Lee, M. C., Xiong, G., Zhang, W., Yang, R., Cieplak, P., Luo, R., Lee, T., Caldwell, J., Wang, J., and Kollman, P. (2003) A point-charge force field for molecular mechanics simulations of proteins based on condensed-phase quantum mechanical calculations. *J. Comput. Chem. 24*, 1999−2012.
(21) Allnér, O., Nilsson, L., and Villa, A. (2012) Magnesium ion-water coordination and exchange in biomolecular simulations. *J. Chem. Theory Comput. 8*, 1493−1502.
(22) Homeyer, N., Horn, A. H., Lanig, H., and Sticht, H. (2006) AMBER force-field parameters for phosphorylated amino acids in different protonation states: Phosphoserine, phosphothreonine, phosphotyrosine, and phosphohistidine. *J. Mol. Model. 12*, 281−289.
(23) Meagher, K. L., Redman, L. T., and Carlson, H. A. (2003) Development of polyphosphate parameters for use with the AMBER force field. *J. Comput. Chem. 24*, 1016−1025.
(24) Berendsen, H. J. C., Postma, J. P. M., van Gunsteren, W. F., and Hermans, J. (1981) Interaction models for water in relation to protein hydration. In *Intermolecular Forces: The Jerusalem Symposium on Quantum Chemistry and Biochemistry* (Pullman, B., Ed.) Vol. *14*, Springer, Dordrecht, The Netherlands.
(25) Ryckaert, J.-P., Ciccotti, G., and Berendsen, H. J. C. (1977) Numerical integration of the Cartesian Equations of Motion of a System with Constraints: Molecular Dynamics of n-Alkanes. *J. Comput. Phys. 23*, 327−341.
(26) Izaguirre, J. A., Catarello, D. P., Wozniak, J. M., and Skeel, R. D. (2001) Langevin stabilization of molecular dynamics. *J. Chem. Phys. 114*, 2090−2098.
(27) Darden, T., York, D., and Pedersen, L. (1993) Particle mesh Ewald: An N-log(N) method for Ewald sums in large systems. *J. Chem. Phys. 98*, 10089−10092.
(28) van Gunsteren, W. F., Billeter, S. R., Eising, A. A., Ḧunenberger, P. H., Kr̈uger, P., Mark, A. E., Scott, W. R. P., and Tironi, I. G. (1996) *Biomolecular Simulation: The GROMOS96 manual and user guide*.
(29) Feig, M., Karanicolas, J., and Brooks, C. L., III (2004) MMTSB Tool Set: Enhanced sampling and multiscale modeling methods for applications in structural biology. *J. Mol. Graphics Modell. 22*, 377−395.
(30) Huse, M., and Kuriyan, J. (2002) The conformational plasticity of protein kinases. *Cell 109*, 275−282.
(31) Kornev, A. P., Haste, N. M., Taylor, S. S., and Eyck, L. F. (2006) Surface comparison of active and inactive protein kinases identifies a conserved activation mechanism. *Proc. Natl. Acad. Sci. U.S.A. 103*, 17783−17788.
(32) Pei, J., Kim, B. H., and Grishin, N. V. (2008) PROMALS3D: A tool for multiple protein sequence and structure alignments. *Nucleic Acids Res. 36*, 2295−2300.
(33) Berteotti, A., Cavalli, A., Branduardi, D., Gervasio, F. L., Recanatini, M., and Parrinello, M. (2009) Protein conformational transitions: The closure mechanism of a kinase explored by atomistic simulations. *J. Am. Chem. Soc. 131*, 244−250.
(34) Bond, P. J., and Faraldo-Gomez, J. D. (2011) Molecular mechanism of selective recruitment of Syk kinases by the membrane antigen-receptor complex. *J. Biol. Chem. 286*, 25872−25881.
(35) Corbi-Verge, C., Marinelli, F., Zafra-Ruano, A., Ruiz-Sanz, J., Luque, I., and Faraldo-Gomez, J. D. (2013) Two-state dynamics of the SH3-SH2 tandem of Abl kinase and the allosteric role of the N-cap. *Proc. Natl. Acad. Sci. U.S.A. 110*, E3372−E3380.
(36) Shan, Y., Seeliger, M. A., Eastwood, M. P., Frank, F., Xu, H., Jensen, M. O., Dror, R. O., Kuriyan, J., and Shaw, D. E. (2009) A conserved protonation-dependent switch controls drug binding in the Abl kinase. *Proc. Natl. Acad. Sci. U.S.A. 106*, 139−144.
(37) Yang, S., Banavali, N. K., and Roux, B. (2009) Mapping the conformational transition in Src activation by cumulating the information from multiple molecular dynamics trajectories. *Proc. Natl. Acad. Sci. U.S.A. 106*, 3776−3781.
(38) Yang, S., and Roux, B. (2008) Src kinase conformational activation: Thermodynamics, pathways, and mechanisms. *PLoS Comput. Biol. 4*, e1000047.